EFFECT OF HEAT TRANSFER THROUGH THE RELEASE PIPE ON SIMULATIONS OF CRYOGENIC HYDROGEN JET FIRES AND HAZARD DISTANCES

Cirrone, D.[1], Makarov, D.[1], Kuznetsov, M.[2], Friedrich, A.[3], Molkov, V.[1]
[1]HySAFER Centre, Ulster University, Newtownabbey, Northern Ireland, BT37 0QB, UK, d.cirrone@ulster.ac.uk, dv.makarov@ulster.ac.uk, v.molkov@ulster.ac.uk
[2]Karlsruhe Institute of Technology, 76131, Karlsruhe, Germany, mike.kuznetsov@kit.edu
[3]Pro-Science, 76725, Ettlingen, Germany, andreas.friedrich@kit.edu

ABSTRACT
Jet flames originated by cryo-compressed ignited hydrogen releases can cause life-threatening conditions in their surroundings. Validated models are needed to accurately predict thermal hazards from a jet fire. Numerical simulations of cryogenic hydrogen flow in the release pipe are performed to assess the effect of heat transfer through the pipe walls on jet parameters. Notional nozzle exit diameter is calculated based on the simulated real nozzle parameters and used in CFD simulations as a boundary condition to model jet fires. The CFD model was previously validated against experiments with vertical cryogenic hydrogen jet fires with release pressures up to 0.5 MPa (abs), release diameter 1.25 mm and temperatures as low as 50 K. This study validates the CFD model in a wider domain of experimental release conditions - horizontal cryogenic jets at exhaust pipe temperature 80 K, pressure up to 2 MPa abs and release diameters up to 4 mm. Simulation results are compared against experimentally measured parameters as hydrogen mass flow rate, flame length and radiative heat flux at several locations from the jet fire. The CFD model reproduces well experiments with reasonable engineering accuracy. Jet fire hazard distances established using three different criteria - temperature, thermal radiation and thermal dose - are compared and discussed based on CFD simulation results.

1. INTRODUCTION

Cryo-compression of hydrogen gas is a competitive technique to store and transport large quantities of hydrogen, due to higher gravimetric and volumetric capacities than compressed gas at ambient temperature [1]. A deep understanding of the consequences resulting from potential accidents with a cryogenic release is of furthermost importance to protect life and prevent property loss for an inherently safer hydrogen infrastructure. The thermal hazards from cryogenic hydrogen jet fires were mainly experimentally investigated. Authors in [2] analysed the thermal radiation emitted by hydrogen ignited releases with pressure up to 3.5 MPa abs and temperature in the range 34-65 K. A maximum radiation level as high as 10 kW/m^2 was recorded at 0.75 m from the jet axis, which is sufficient to provoke second-degree burns after 20 s exposure according to published harm criteria [3]. Sandia National Laboratories (SNL) performed experiments on cryogenic jet fires with release temperature down to 37 K and pressures up to 0.6 MPa abs [4]. Experimental measurements showed an increase of radiative heat flux for decreasing release temperature at a given mass flow rate.

The heat transfer through the wall of a release pipe exposed to ambient temperature and connecting the storage system to the nozzle affects the cryogenic flow characteristics. For instance, the heat transfer from cold gas inside the vessel to the ambient air under high pressure release at 200 bar leads to bulk temperature increase in 50 and 175 degrees for 4-mm and 2-mm nozzle respectively [5]. Of course, it changes an iso-entropy of flow characteristics and even the state of the gas from liquid to the gaseous one. The first part of the present study assesses the effect of heat transfer using computational fluid dynamics (CFD) simulations. The study will then analyse the capability of a notional nozzle theory applied to cryogenic under-expanded jets by using the parameters obtained at the real nozzle exit by the CFD simulations. The notional nozzle parameters are implemented as an input into the CFD simulations of hydrogen jet fires. The CFD model previously developed by the authors and validated against SNL vertical hydrogen jet fires with release pressure up to 0.5 MPa abs and temperature in the range 48-82 K is employed to expand the validation domain to horizontal jet fires with higher storage pressure and larger nozzle diameter [6]. Experiments performed at Karlsruhe Institute of Technology (KIT) on ignited

hydrogen releases at the temperature 80 K and pressure 0.3-2.0 MPa were used for validating the CFD model by comparison with the measured radiative heat flux and the flame length.

Predictive engineering tools are available in the literature to calculate hazard distances from the momentum-dominated hydrogen jet fires using the flame length correlation [7]. The "fatality" limit condition is achieved at a axial distance (x) equal to the twofold flame length ($x = 2L_f$), the "pain" limit at x=3L_f and the "no harm" limit at x=3.5L_f. Such distances were defined for vertical jet fires. In horizontal jet fires, combustion products will raise because of buoyancy. This may lead to reduction of hazard distances along the original jet axis. Engineering tools able to predict the resulting harm level are practically missing, as well as tools to estimate thermal hazards aside of the jet fire. The thermal dose is well suited for this purpose, as it takes into account both the exposure duration and the radiative heat flux. Experimental work [8] on jet fires from a 60 l/min liquid hydrogen (LH_2) spillage concluded that distance greater than 8.7 m from the jet fire (L_f=5m) should be maintained to avoid a harmful thermal dose of 92 $(kW/m^2)^{4/3}s$ for an exposure time up to 200 s. A time of 28 s was found sufficient to reach the pain limit at 7.6 m. The computational study [9] concluded that for tests with temperature 48-78 K and pressure 0.2-0.4 MPa abs from 1.25 mm nozzle, people at 0.5 m from the jet fire axis should stand less than 30 s to not incur in first degree burns.

The present study aims at the validation of the CFD model accounting for the effect of heat transfer in the release pipe on flow parameters and assessing thermal hazard distances for horizontal cryogenic jet fires with release pressure and diameter up to 2 MPa and 4 mm respectively. The analysis is focused on distributions of temperature, thermal radiation and thermal dose along and aside of the jet axis. The horizontal jet fire and combustion products may be affected by buoyancy, causing the tilting of the flame axis. For this reason, the study distinguishes the release direction from the flame tilted axis.

2. DESCRIPTION OF VALIDATION EXPERIMENTS

Experiments on cryogenic hydrogen jet fires were performed at the ICESAFE facility of Karlsruhe Institute of Technology (KIT) in Germany [10]. Hydrogen was released horizontally at a height of 0.9 m inside a 160 m^3 chamber with dimensions 8.5x3.4x5.5 m. The facility was designed for quasi-steady-state release conditions, with constant release temperature and pressure. Figure 1a shows a schematic of the release system used in the experiments. Hydrogen flow temperature and pressure were measured at the location marked as "cross". Hydrogen conditions at the "cross" are taken as representative of hydrogen storage conditions. Afterward, the gas flows in a pipe of unknown length, then through a valve and finally in a 60 mm pipe before the discharge into the atmosphere. The pipe has an inner diameter equal to 10 mm and an outer diameter of 12 mm. The geometry and dimensions of the pipe are shown in Fig. 1b. Overall, six tests were performed for different temperatures, pressures and release diameters. Table 1 shows the operating conditions for six experiments. The nozzle diameter is *D*=2 mm for Tests 1, 3 and 4, and *D*=4 mm for Tests 2, 5 and 6. Two test series were performed for hydrogen at ambient temperature (290 K). Four tests were performed with cryogenic hydrogen (80 K). The tests at ambient and cryogenic temperatures are used to analyse the release modelling capabilities. The CFD modelling of jet fires is focused on the four tests with hydrogen at cryogenic temperature, as it is the main objective of the study. The jet was ignited after 2 s of the release to establish the steadiness of the process. Ignition was triggered at 0.4 m from the release point and had a duration of 400 ms. The jet flame duration was 8 s to reach saturation of the radiative heat flux at the sensors. Two different sensors were available and were located as a pair at each given position. One sensor had no window with an optical filter and recorded the full spectrum of incident radiation (indicated as NW). A second sensor had a ZnSe filter in the window to record the incident radiation with wavelengths in the range 0.5-22 μm, which includes the range 2-9 μm for steam radiation (indicated as ZnSeW). In the tests, the sensors were located at the same height as the jet fire (0.9 m) and were moved in nine steps of 0.25 m distance on a movable support parallel to the release direction. For each position, a separate test with exactly the same release conditions was performed. In the first series, the support was located at distance 0.5 m from the release direction, in two further test series the sensors support was moved to 0.75 m and then 1.25 m from the jet axis to permit measurements with increasing distance from the jet fire. Figure 1c shows the location of radiometers with respect to the jet flame and reports the univocal denomination for each sensor

configuration (every symbol corresponds to one test with both sensors in the respective position). The flame length (L_f) was experimentally determined as $\frac{X_{Q,max}}{0.6}$, where $X_{Q,max}$ is the distance at which the maximum radiative heat flux was recorded. This consideration is consistent with observations on the distance along the jet axis where the highest temperature is recorded: $X_{T,max} = 0.6L_f$ [11].

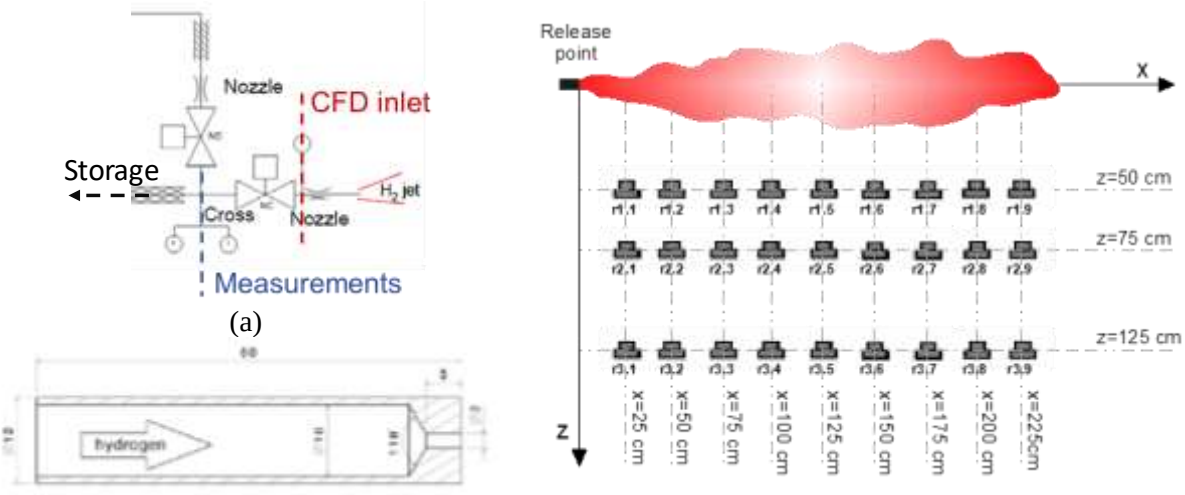

Figure 1. a) experimental release system; b) drawing of the pipe section with the nozzle (dimensions in mm) [10]; c) top view of the experimental set-up for thermal radiation measurements at height 0.9 m.

3. RELEASE SOURCE MODELLING

Experimental bulk pressure was in the range 0.3-2 MPa abs (Table 1). Thus, jets were under-expanded with pressure at the real nozzle exit being higher than atmospheric. The expansion of the flow to ambient pressure is characterised by shock waves and supersonic velocities. An accurate resolution of this zone requires higher refinement and complex numerical codes. The alternative and widely used notional nozzle theory is employed to model the release sources in the jet fires simulations [6, 11]. The flow at the notional nozzle exit has expanded to ambient pressure and has a uniform sonic velocity.

Table 1. Experimental conditions of the validation tests [10]. Pressure and temperature are measured at the "cross" upstream a valve and 60 mm release pipe (see Fig. 1a). Notional nozzle exit parameters.

Test No.	**1**	**2**	**3**	**4**	**5**	**6**
Experimental operating conditions						
Pressure, MPa abs	2.0	0.4	1.4	2.0	0.3	0.4
Temperature, K	290	290	80	80	80	80
Real nozzle diameter, mm	2	4	2	2	4	4
Experimental mass flow rate, g/s	3.3	3.3	3.3	4.4	3.3	4.4
Notional nozzle exit parameters						
Temperature, K	241.7	241.7	66.7	66.7	66.7	66.7
Velocity, m/s	1181.3	1181.3	620.4	620.4	620.4	620.4
Density, kg/m^3	0.102	0.102	0.369	0.369	0.369	0.369
Calculations without a discharge coefficient C_D						
Notional nozzle diameter, mm	6.43	5.77	5.35	6.36	4.99	5.76
Calculated mass flow rate, g/s	3.90	3.14	5.13	7.27	4.47	5.95
Deviation of calculated mass flow rate from experiment, %	15.4	-5.1	35.7	37.3	26.2	26.0
Calculations with the inclusion of a discharge coefficient C_D						
Defined discharge coefficient	0.85	1	0.64	0.6	0.74	0.74
Notional nozzle diameter, mm	5.93	5.77	4.3	4.93	4.3	4.96
Calculated mass flow rate, g/s	3.3	3.14	3.3	4.4	3.3	4.4

3.1 Notional nozzle approach and discharge coefficient application

The under-expanded jet theory [12] represents well cryogenic hydrogen releases with the temperature down to 46 K and pressure up to 0.6 MPa ([6,13]). This theory uses Abel-Noble Equation of State (EOS) to account for the non-ideal behaviour of hydrogen gas at high pressure. The theory assumes an isentropic expansion from the stagnation pressure in a storage vessel through the real nozzle and, finally, after the jet expansion to the atmospheric pressure through the notional nozzle exit. The equations for energy and mass conservation are employed in an assumption of a sonic flow to calculate conditions at the notional nozzle exit. Table 1 shows the calculated notional nozzle exit parameters and mass flow rate assuming adiabatic (no heat exchange) flow conditions. Mass flow rate for warmer releases is reasonably predicted within ±15% accuracy. On the other hand, the mass flow rate for cryogenic releases is significantly overestimated up to 37% for Test 4. A discharge coefficient, C_D, can be introduced in calculations to match the experimental flow rate. The discharge coefficient is a dimensionless number and generally its value is affected by friction and minor losses in the release path and possible non-zero velocity of the gas in the storage vessel. Table 1 presents the calculated notional nozzle parameters applying the discharge coefficient. Test 3 (D=2mm) and Test 5 (D=4mm) would result in the same notional nozzle characteristics to be imposed in CFD simulations, and hence in same jet fires. Similar observations can be done for Test 4 (D=2mm) and Test 6 (D=4mm). However, experiments demonstrated that the larger release diameter results in the higher radiative heat flux and the longer flame lengths. Thus, it can be concluded that the simple application of the discharge coefficient to match the experimental mass flow rate is not sufficient to correctly simulate a cryogenic release, as not capable to catch the variation in release conditions due to the presence of heat transfer even if the mass flow rate could be met exactly. Therefore, a different approach is used.

3.2 Numerical simulations of cryogenic hydrogen flow in the release pipe

CFD simulations are performed to characterise hydrogen flow parameters accounting for heat transfer between the cryogenic flow and the pipe wall. Hydrogen conditions measured at the "cross" as in Table 1 are taken as the inlet boundary conditions in the CFD simulations of hydrogen flow in the 60 mm pipe (see Fig. 1a). The schematic of the pipe geometry and dimensions are shown in Fig. 1b. The CFD model uses an LES explicit density-based solver. The dynamic Smagorinsky-Lilly sub-grid scale model is applied for turbulence [14]. The time step is dictated by a Courant-Friedrichs-Lewy number equal to CFL=0.9. The specific heat of hydrogen is defined as a polynomial function interpolating NIST data for cryogenic temperatures [15]. The numerical domain is cylindrical with a radius of 70 mm and axial length of 180 mm. The release nozzle is discretized with 13 cells along the diameter, as suggested in [16], leading to an average cell size of 0.15 mm for the 2 mm nozzle. The numerical grid has 263,110 control volumes (CV). The solid pipe walls are discretized with 19 cells in the radial direction to model the conductive heat transfer through them. Steel properties are 8030 kg/m^3 for density, 502.48 J/kg/K for specific heat and 16.27 W/m/K for thermal conductivity [17]. The details of the release pipe geometry and a "zoom in" of the grid in the pipe near field are shown in Fig. 2.

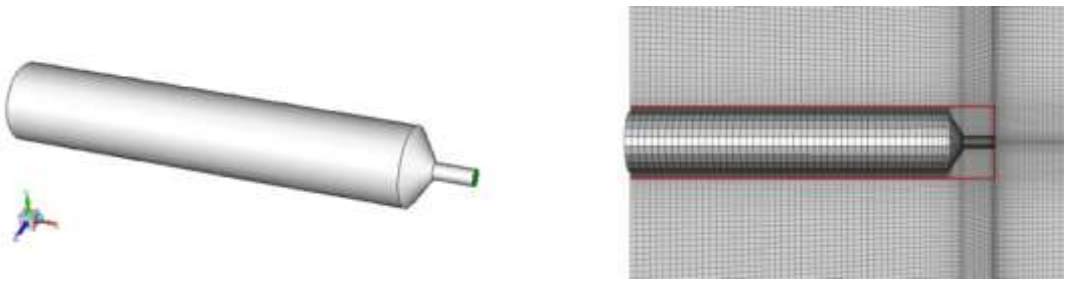

(a) (b)

Figure 2. a) geometry of the internal walls of the release pipe; b) the numerical grid of the pipe internal walls, the outline of the pipe external walls (red solid lines) and mesh in the pipe near field.

A pressure inlet condition is imposed at the pipe entrance. External boundaries are pressure outlets with gauge pressure equal to 0 and a temperature of 288 K. Air composition is 0.21 oxygen and 0.79 of nitrogen by mole fraction. The 2nd order upwind scheme is used for the flow spatial discretization.

3.2.1. Results and discussion

A first assessment of the effect of heat transfer through the pipe walls is conducted for Test 3. Figure 3a shows a comparison of mass flow rate at the real nozzle exit for adiabatic and non-adiabatic pipe walls. The hydrogen flow stabilises during 2-7 ms, as confirmed by the constant flow beyond this time. Figure 3b shows the radial distribution of temperature at an axial distance of 50 mm, i.e. in the ending section of the pipe with the inner diameter 10 mm for the time 12 ms. It can be observed that temperature at the axis is the same for both the cases, however, radially, the inclusion of heat transfer causes an increase of temperature of the fluid towards the wall at 5 mm radial distance, reaching almost 150 K in the layer of cells closer to the wall. Similarly, the temperature at the nozzle exit is not uniformly distributed (see Fig. 4). The temperature in the core of the flow is approximately 57 K and it rapidly increases towards the tube walls up to 105 K due to heat transfer. Therefore, the temperature averaged by the nozzle cross area is considered in this case. When the heat transfer through the walls is included in simulations (non-adiabatic walls), the calculated established mass flow rate is 4.25 g/s and the temperature of hydrogen at the nozzle exit is about 72 K. The heat transfer rate through the wall is equal to 754 W, 75% of which goes through the pipe of wider diameter 10 mm. If the heat transfer through the wall is not included, the hydrogen mass flow rate is approximately 9% higher (4.65 g/s) and the temperature of the flow is lower (56 K).

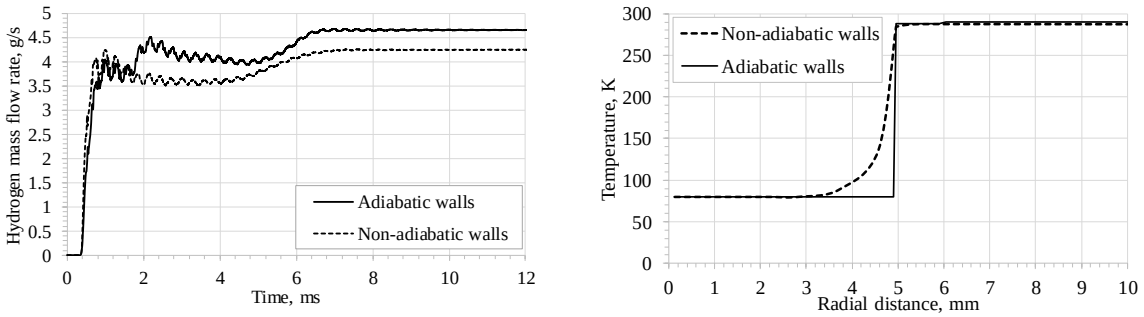

(a) (b)

Figure 3. Effect of heat transfer through the pipe walls (non-adiabatic vs adiabatic walls) for Test 3: (a) hydrogen mass flow rate; (b) temperature radial distribution at 50 mm axial distance at 12 ms.

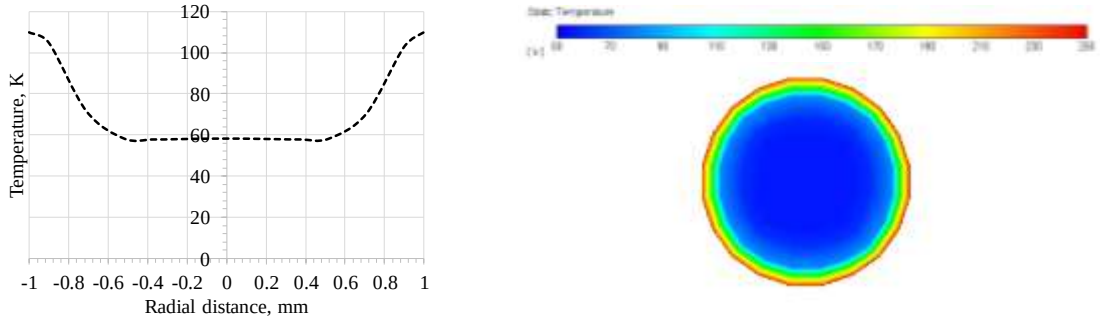

(a) (b)

Figure 4. Temperature distribution at the real nozzle exit at 12 ms: non-adiabatic pipe walls for Test 3.

A mesh sensitivity analysis is performed by halving the cell size in the zone (12x120 mm) that includes the release pipe and surrounding near zone. The resulting mesh has 943,265 CVs. The mesh refinement causes an increase by 7.6% of the integral heat flux through the pipe walls for Test 3. The maximum relative difference in the calculated mass flow rate is 3.8%, whereas it is negligible for the other parameters at the nozzle, e.g. temperature. Thus, it is concluded that the level of accuracy of the solution is acceptable compared to the gain in computational time required by calculations.

Simulations are performed for the remaining three tests with cryogenic hydrogen by changing the inlet pressure and numerical grid for the respective release nozzle. Table 2 shows the resulting flow parameters at the real nozzle exit. It can be observed that the discrepancy between simulated and experimentally measured mass flow rates increases with the inlet pressure, reaching almost 30% for Test

4 at the highest inlet pressure (2.0 MPa). As shown in Table 2, higher pressures are associated with larger heat transfer in the pipe, due to a higher velocity of the flow and thus higher convective heat transfer between hydrogen and the pipe. As shown in Fig. 1a, the hydrogen temperature and pressure (hereby considered as inlet conditions for the CFD simulations) were measured somewhere upstream of the simulated release pipe. From the measurement location to the actual inlet of the 60 mm pipe, the cryogenic hydrogen gas flows in a pipe of unknown length and through a valve. The authors believe that the cause of discrepancy in the calculated mass flow rate is to be looked for in the heat transfer taking place in the release system between the measurement location and the 60 mm pipe.

Table 2. Parameters at the real nozzle calculated from CFD modelling including conjugate heat transfer through the 60 mm pipe walls.

Test No.		**3**	**4**	**5**	**6**
Inlet	Temperature, K	80	80	80	80
	Pressure, MPa	1.4	2	0.3	0.4
Real nozzle exit	Diameter, mm	2	2	4	4
	Temperature, K	71.4	70.7	75.9	73.3
	Pressure, MPa	0.499	0.705	0.122	0.160
	Velocity, m/s	798.7	801.2	746.1	750.9
	Density, kg/m^3	1.798	2.566	0.423	0.570
	Calculated mass flow rate, g/s	4.25	6.10	3.88	5.2
	Variation of calculated mass flow rate from experiment, %	22.4	27.8	15.0	15.4
Pipe wall	Total surface heat transfer rate, W	754.4	973.2	680.0	794.9

3.2.2. Adjustment of inlet conditions

In this section, the inlet temperature is modified to include the effect of heat transfer in the release system upstream of the 60 mm release pipe ending with the real nozzle. Inlet temperature has been gradually increased by +10 K value until the best fit with the experimental mass flow rate is found. Table 3 shows the resulting parameters at the real nozzle exit. This is considered to be a rational procedure to estimate the flow characteristics, showing that the inclusion of heat transfer in just 60 mm pipe for Test 3 is capable to cause an increase of temperature by 16 K at the real nozzle exit. A longer pipe, as present between the sensor location and the nozzle, may result in a larger temperature difference. As expected, releases at higher pressure result in a higher inlet temperature because of the expected higher heat flux.

Table 3. Parameters at the real nozzle exit calculated from CFD simulations including conjugate heat transfer through the pipe walls and inlet temperature modification.

Test No.		**3**	**4**	**5**	**6**
Inlet	Temperature, K	140	150	110	110
	Pressure, MPa	1.4	2	0.3	0.4
Real nozzle exit	Diameter, mm	2	2	4	4
	Temperature, K	120.7	126.7	100.0	98.4
	Pressure, MPa	0.549	0.788	0.127	0.168
	Velocity, m/s	967.5	989.2	835.9	844.7
	Density, kg/m^3	1.12	1.52	0.322	0.43
	Calculated mass flow rate, g/s	3.28	4.55	3.34	4.47
	Variation of calculated mass flow rate from experiment, %	-0.6	3.6	1.2	1.6

The CFD simulations of the hydrogen flow in the release pipe allow calculating the flow characteristics at the real nozzle exit taking into account the effect of conjugate heat transfer through the release pipe. The simulated parameters are used to estimate the flow characteristics at the notional nozzle exit where the gas has fully expanded to ambient pressure. The flow is assumed to expand isentropically between the real nozzle and the notional nozzle exit. The equations for mass and energy conservation, along with

the assumption of uniformly sonic speed, are used to estimate parameters at the notional nozzle exit, including its diameter. Table 4 shows the calculation results that will be used as inlet conditions in numerical simulations of the hydrogen jet fires.

Table 4. Calculated notional nozzle exit parameters accounting for the effect of conjugate heat transfer in the release pipe and hydrogen path downstream to the location "cross" with measured temperature and pressure.

Test No.	**3**	**4**	**5**	**6**
Temperature, K	120.6	126.8	99.4	97.7
Velocity, m/s	834.4	855.6	757.4	751.0
Density, kg/m^3	0.204	0.194	0.247	0.252
Diameter, mm	5.0	6.0	4.8	5.6

4. JET FIRE MODELLING

4.1. The CFD model of hydrogen jet fire

The CFD model employed here was previously validated against vertical cryogenic hydrogen jet fires and described in paper [6]. ANSYS Fluent is used as a software platform. Numerical simulations employ a pressure-based solver and so called "incompressible ideal gas" assumption for the flow (i.e. density calculation based on constant pressure and variable temperature). A Reynolds-Averaged Navier-Stokes (RANS) approach is used to resolve conservation equations for mass, momentum, energy and species. A turbulent Schmidt number, Sc_t, equal to 0.9, is used in the governing equations. Realizable k-ε model of turbulence is applied [18], by solving the transport equations for turbulence kinetic energy, k, and turbulent dissipation rate, ε. Combustion is modelled through the Eddy Dissipation Concept (EDC) model [19]. The CFD model includes detailed chemical mechanisms for hydrogen combustion in air through 18 elementary reactions and 9 species [20]. Radiation is modelled through the Discrete Ordinates (DO) model [21]. A refinement of 10x10 rays and 3x3 pixels is employed for discretising the radiative transfer equation (RTE) as suggested in [6]. The RTE solved through the DO model is updated every 200 flow iterations to reduce calculation time and maintain good solution accuracy (maximum 0.1% variation). For hydrogen combustion in air, the only emitting and absorbing specie is water vapour, hereby considered as a grey gas. A function of Planck absorption coefficient on temperature and H_2O partial pressure interpolating Hubbard and Tien's data available in [22] is used in the study. Simulations are steady-state, as they aim at modelling established jet fires with constant release conditions. Convective terms in governing equations are discretised with a second-order upwind scheme, and a SIMPLE approach is used for velocity-pressure coupling.

4.2 Computational domain and numerical details

A domain with the same size as the test chamber (8.5x3.4x5.5m) is considered. The overall domain counts 1,322,921 CVs. The numerical grid is hexahedral. Figure 5a shows the numerical grid on the plane in the vertical cross section at z=0, parallel to the hydrogen jet direction. The release pipe is assumed to have a length equal to 10 cm and the same cross-section as the notional nozzle exit, located at a 0.5 m distance from the domain boundary behind it. The nozzle is modelled as one square cell with an area equivalent to that of the round notional nozzle exit (see diameter in Table 4). Thus, the minimum cell size in the numerical grid is the length of the square release for each test, e.g. 4.5 mm for Test 3. A maximum cell growth ratio of 1.1 is set in proximity of the jet fire. The details of the numerical grid in the proximity of the release point are shown in Fig. 5b. Radiometers are modelled as 2x2 cm square surfaces, located as in the experiments (see Fig. 1). The cell size in the jet fire zone and between the radiometers is maintained equal to 2 cm. The lateral and top external boundaries of the domain are modelled as pressure outlet with gauge pressure equal to 0. The floor is defined as an adiabatic wall with emissivity 0.6, as indicated for steel in [23]. The notional nozzle exit is modelled as a velocity inlet, with parameters as defined in Table 4. A turbulent intensity of 25% and turbulent length scale equal to $0.07D_{not}$ are set at the inlet, following the conclusions of the study [6]. Radiometers are modelled as non-slip and isothermal surfaces with emissivity 1, to prevent radiation reflection and to take into account the entire incident radiation. As the initial conditions, the temperature was equal to 288 K and

relative humidity equal to 77%, which is the average annual value recorded in the location of experiments [24]. These conditions are set for the entraining air at the external boundaries. Simulations are performed as well for a relative humidity of 50%, which is generally suggested for controlled environments, e.g. laboratories and testing facilities.

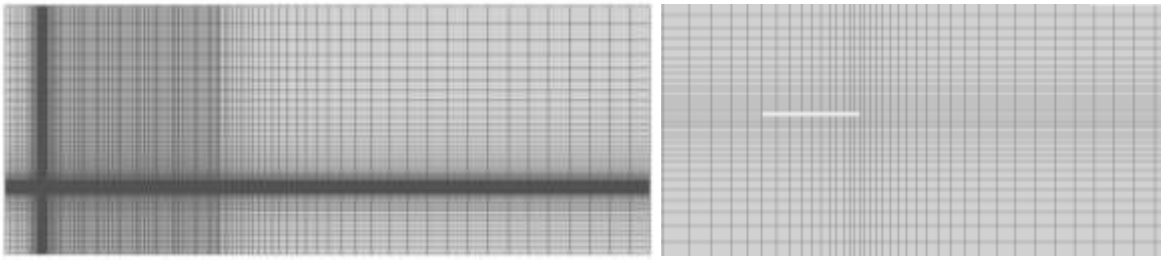

(a) (b)

Figure 5. a) view of the numerical grid in plane z=0; b) zoomed-in view in the release proximity.

4.3 Results and discussion

Simulations of jet fires are performed for all four tests on cryogenic releases. Comparison with experiments is performed for the radiative heat flux measured at the sensors and the jet fire flame length. Figure 6 shows the resulting distribution of temperature, water vapour and hydroxyl (OH) mole fraction in the entire domain for Test 3. It can be observed that distributions of temperature and water vapour are affected by buoyancy which can qualitatively lead to a decrease of thermal hazard distances from the jet fire. The OH mole fraction distribution gives insights into the zone of the jet fire mainly involved in the combustion reaction. The flame is characterised by a tilted axis, due to buoyancy affecting the terminal portion of the jet. This somewhat differs from the experimental observation that the flame is momentum-dominated. The authors believe that this may be due to the use of the notional nozzle in simulations, which models the jet as sonic with uniform velocity. This may cause a different velocity decay in the jet leading to an effect of buoyancy over momentum forces and the deflection of the jet axis. This effect was experimentally observed in large scale jet fires [25].

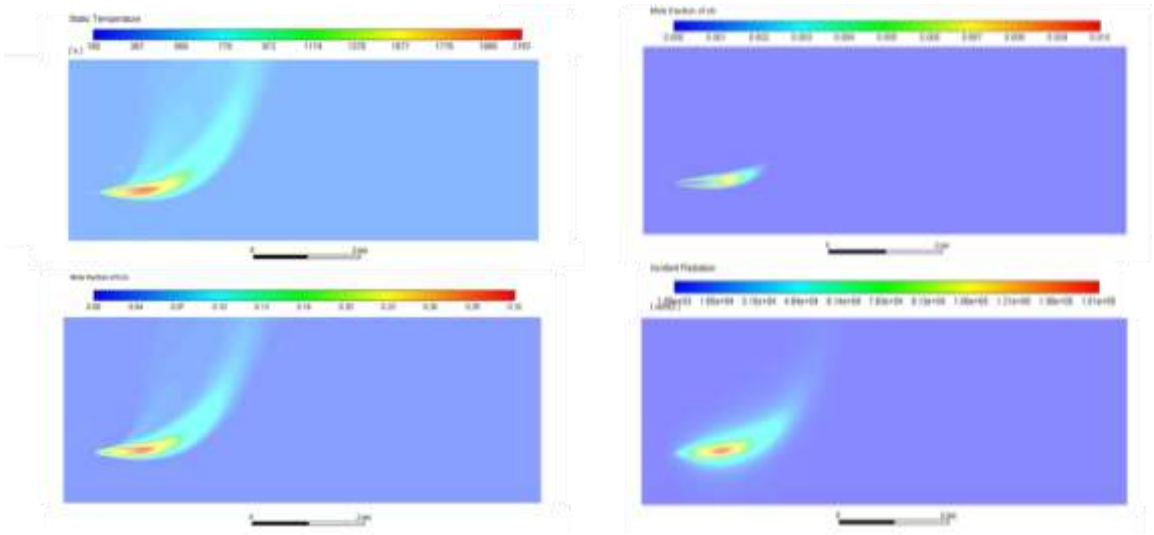

Figure 6. Distribution of temperature, H2O and OH mole fraction, incident radiation for Test 3 (z=0).

Figure 7 shows the calculated radiative heat flux for relative humidity (Rh) 77% and 50% versus experimental measurements at sensors for Tests 3 and 4 (D=2 mm). Experimental records by both of the two radiometers typologies, i.e. through NW and ZnSeW windows, are reported for comparison. Diamonds for each curve represent the records at 9 sensors located on the same line parallel to the release direction and shown in Fig. 1c. Test 3 simulation for Rh=77% well reproduces experimental radiative heat flux at sensors at 50 cm and 75 cm from the axis with 10% accuracy. The exception is given by sensors r1.5, r1.7 and r1.9, where a maximum variation of +25% is reached. However, simulation results underestimate experiments for the line of sensors at z=125 cm (r3.1-3.9), reaching a maximum variation

of 30% towards the central zone of the jet fire. Similar observations can be made for Test 4. Radiative heat flux is predicted with an accuracy within 20% for the sensors located at distances 50 and 75 cm from the jet axis (r1.1-r1.9, r2.1-r2.9). On the other hand, simulation presents an underestimation up to 40% for the sensors at a distance of 125 cm from the axis (r3.1-r3.9). Several tests were performed ensuring same release pressure and temperature to measure the radiative heat flux at different distances from the jet by moving the sensors' support. Therefore, a possible decrease of pressure in between tests due to the storage tank blowdown may be excluded from the possible causes of underestimation of simulated radiative heat flux at 1.25 m distance. Figure 7 includes results of simulated radiative heat flux for Rh=50%. The relative difference between cases with Rh=50% and 77% increases with distance from the jet axis, varying from 16% for the sensors r1.1-r1.9 at 50 cm from the jet to 27% for sensors r3.1-r3.9 at z=125 cm. For both Tests 3 and 4, simulated radiative heat flux with Rh=50% overlaps with experiments at the further distance from the jet axis, conversely to the underestimation observed with Rh=77%. It is believed that actual relative humidity is in the range 50-77%, chosen as representative scenarios for the analysis. It should be underlined that in between experiments, the test chamber was ventilated to remove combustion products and provide fresh air. In case of not total removal, the actual relative humidity could have been different from range 50-77%.

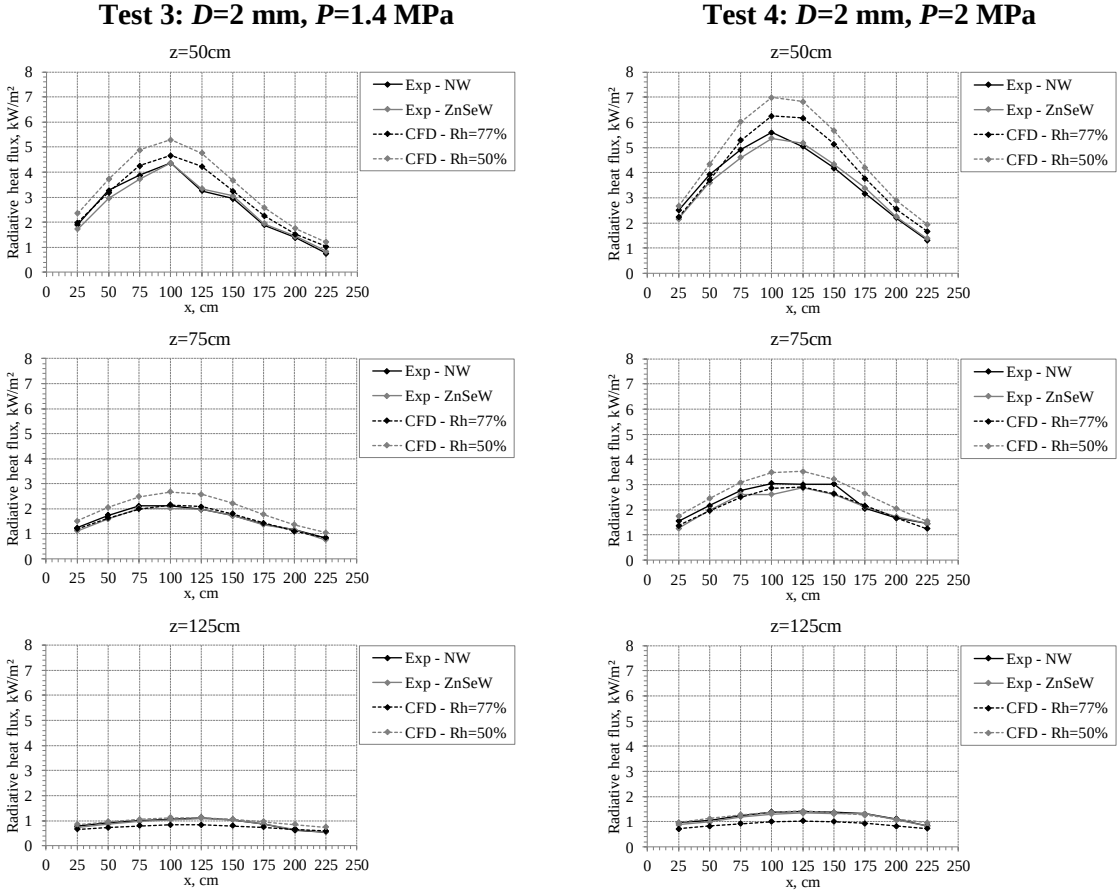

Figure 7. Comparison of experimental and simulated radiative heat fluxes for Test 3 and Test 4.

Simulations of Test 5 with Rh=77% well predict the experimental radiative heat flux for the ZnSeW sensors r1.1-r1.9 at 50 cm distance from the jet axis (see Fig. 8). At further distances, simulations underpredict experimental measurements, up to about 40% at z=125 cm. Simulations employing a Rh=50% get closer to experiments (17% variation). Simulations of Tests 6 (Rh=77%) agree well with experimental measurements at sensors r1.1-r1.4 located closer to the release (x up to 100 cm). Beyond this point, a significant variation is recorded, mainly oriented towards an underestimation of experimental measurements. This is consistent with the underprediction of flame length and thus the zone emitting radiation (see Table 5 below). Generally, it could be observed a worsening in predictive capability for a larger release diameter (4 mm) when the Rh=77% is considered. This may be due to

lower relative humidity in the chamber for these tests. Furthermore, assuming a uniform sonic velocity at the nozzle may well approximate conditions for smaller diameters (D=2 mm), but may weaken for larger diameters (D=4mm) due to the effect on spreading rate of the jet. Finally, it has been observed that different nozzle shapes may affect the angle of the jet in the nozzle near field.

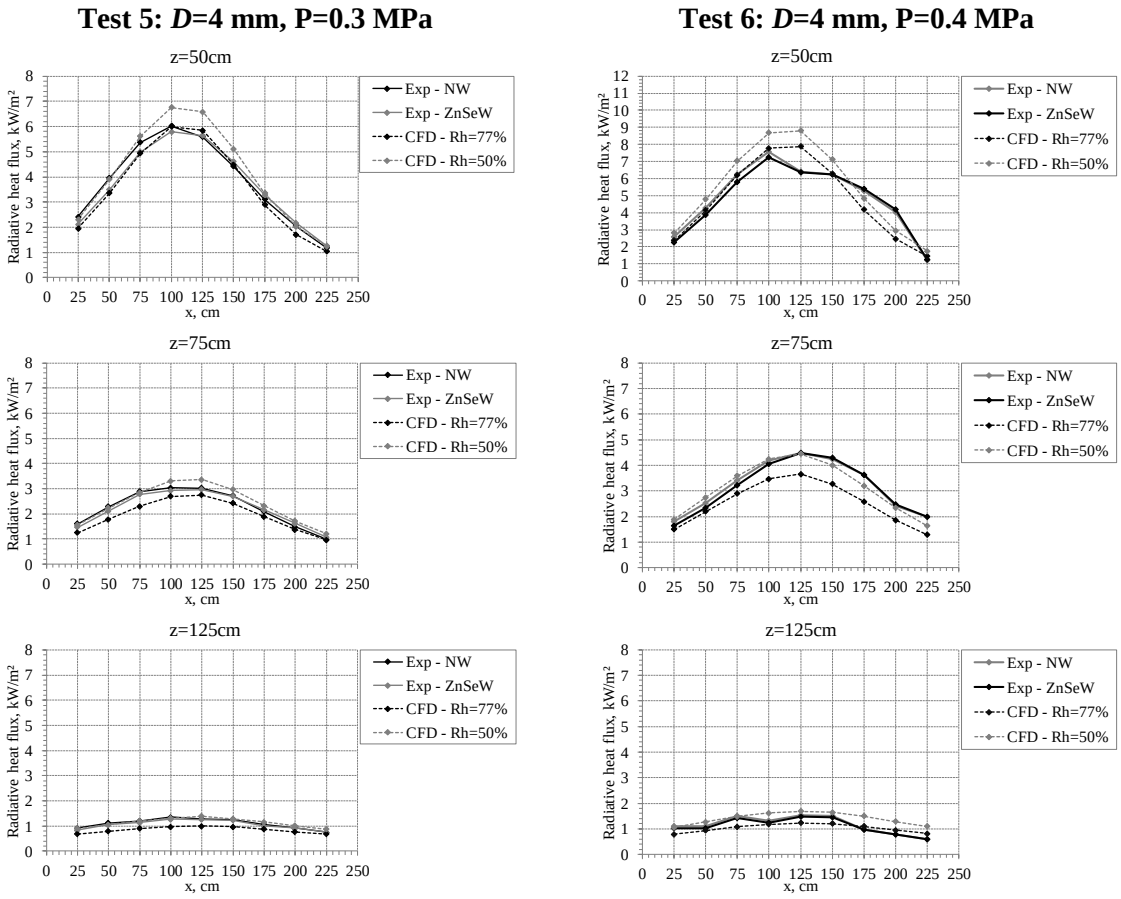

Figure 8. Comparison of experimental and simulated radiative heat fluxes for Test 5 and Test 6.

As widely discussed in the literature, an accurate estimation of flame length for hydrogen jet fires is not a trivial task, neither in experiments nor simulations. Thus, analysis of flame length shall be handled carefully and with the awareness about associated accuracy level. In simulations, a region with temperature in the range 1300-1500 K was considered to correspond to the visible flame length [26]. Further criteria was the limit to OH mole fraction equal to 0.001 to indicate the most reacting zone based on work in [27]. Table 5 shows the experimental and simulated flame lengths, which was calculated as the further x coordinate along the tilting jet axis from the release where the criteria were met, due to buoyancy effects on the flame. Overall, simulations well predict the experimental flame length for Tests 3, 4 and 5. The largest difference, yet within acceptable 15%, was observed for Test 6.

Table 5. Comparison of experimental and simulated flame lengths.

Test	**3**	**4**	**5**	**6**
Experiment, m	1.66	1.83	1.62	2.08
CFD 1300 K, m	1.68	1.89	1.72	1.86
CFD 1500 K, m	1.51	1.70	1.57	1.70
CFD $mf_{OH} = 0.001$, m	1.60	1.81	1.65	1.79

4.3.1. Convergence and sensitivity of numerical simulations

Simulations are steady-state type. A solution was considered converged when the axial distributions of temperature, H_2O and OH mole fractions, velocity, and the radiative heat flux at the sensors did not change with the advancement of iterations. Convergence was reached at 15,000 iterations and required

about 20 hours to calculate on a 62 CPU machine. A mesh sensitivity analysis was conducted on Test 3 (Rh=77%) to ensure grid independence of simulations. The CV size is halved at the nozzle, the jet fire area and its surroundings up to the sensors. The refined grid has 4,372,060 CVs. Calculation time for 1,000 iterations raises from about 1.4 h to 5 h for the finer mesh. Relative maximum variation of radiative heat flux decreased from 8% for the sensors line at 50 cm from the jet axis to 4% at 75 cm, and to less than 2% at 125 cm. A variation of 3% was recorded on the simulated flame length. Overall, these deviations are considered acceptable concluding that there is numerical grid convergence. The effect of ground emissivity was assessed by increasing it from 0.6 to 1, which means total absorption of incoming radiation. Radiative heat flux varied by 1% for the sensors located at 50 cm from the jet axis, and by 3% for those located at 75 cm. It is concluded that the ground emissivity has a negligible effect on the radiation recorded in the proximity of the jet fires. As observed in Figs. 7-8, simulated radiative heat flux at sensors strongly depends on the water vapour content in the air. Assumption of dry air in absence of exact experimental data may result in a significant overestimation of simulated radiative heat flux in the surroundings of a jet fire, due to the absence of absorption of energy by the water vapour in the air. Results from simulation of Test 3 with dry air assumption (Rh=0%) causes an increase of recorded radiative heat flux by approximately 1.7 times at 50 cm and up to 3 times at 125 cm distance compared to the case with Rh=77%, overestimating significantly experiments and leading to the conclusion that dry air assumption in numerical simulations is far from reality.

4.3.2. Hazard distances for cryogenic horizontal jet fires

The jet flame affects the temperature in its surroundings, producing hot air currents harmful to people. The experimental data on temperature distribution along a hydrogen jet flame trajectory measured in [11,28,29] were analysed in [6]. The study [6] correlated the temperature distribution as a function of the axial distance from the release point (x) normalised by the flame length L_f, to derive the following hazard distances using published harm criteria for people:

- "No-harm" hazard distance (70°C for any exposure duration): x=3.5L_f;
- "Pain" hazard distance (115°C for 5 minutes exposure): x =3L_f;
- "Fatality" hazard distance (309°C, third-degree burns for 20 s exposure): x =2L_f.

These hazard distances are referred to vertical jet flames. Temperature distribution and associated hazard distances may change for horizontal jet fires because of combustion products' buoyancy. The CFD model showed to well represent radiative and flame length characteristics, hence, it is presumed that it well represented distribution of hot combustion products too. Figure 9 shows the calculated temperature along the release direction at a height of 0.9 m, i.e. the height of the release. Distribution is reported as a function of the distance normalised to the flame length calculated according to the temperature criterion (1300-1500 K). The temperature distribution for vertical and horizontal jet fires is similar within the jet fire for distances lower than x=0.6 ÷ 0.7L_f. Beyond this distance, the temperature rapidly decreases along this horizontal line reaching ambient temperature already within x=1.2L_f. Indeed, the effect of buoyancy was seen already towards the tip of the flame, causing a rapid rise of hot combustion products. Considering the flame length calculated by 1500 K limit, maximum distances to the harm thresholds are seen to decrease as follows along the release direction at height 0.9 m: "fatality" distance at x=1L_f; "pain" limit at x=1.1L_f; "no harm" limit at x=1.15L_f.

However, the maximum temperature at a certain distance from the release point may not be located in the release direction due to the effect of buoyancy on combustion products (see Fig. 6). Thus, a second analysis is performed to retrieve the maximum temperature recorded at any height y up to 3.4 m for a certain distance x through Matlab software. Figure 9 (dashed curves) shows the retrieved maximum temperature as a function of the distance x normalised by the flame length for distances approximately x>0.5L_f, where buoyancy started to cause tilting of the jet fire axis. Temperature distributions for the horizontal and vertical jet fires show similar trends up to x=1.5L_f. Beyond this point, it can be seen that a horizontal jet fire shows a faster decrease in the maximum temperature with the distance x from the release. The criterion of 1500 K for the flame length in CFD simulations is considered in the following statements. The hazard distances according to harmful temperature criteria can be calculated as follows:

"fatality" limit at x=1.75L_f; "pain" limit at x=2.1L_f; "no-harm" limit at x=2.2L_f. The latter normalised distance corresponds to 3.3 m from the release point. Ambient temperature is reached at the horizontal distance x=2.3L_f. Similar results are obtained for the remaining three tests, with exception of Test 6 where "no-harm" distance is slightly reduced to x=2.0L_f. It may be concluded that hazard distances for hot air currents as defined for vertical jet fires may be too conservative if applied to horizontal jet fires. It should be highlighted that these distances are referred to the open space.

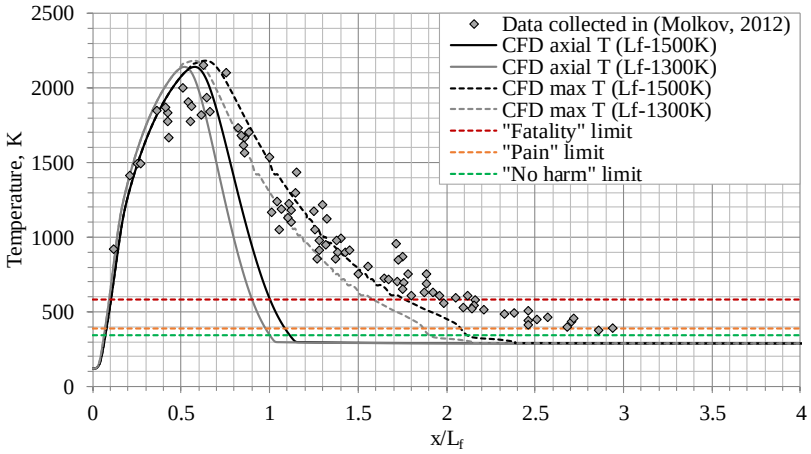

Figure 9. Temperature as a function of distance normalised to flame length (L_f) for vertical jet fires experiments [7] (diamonds) and simulated horizontal jet fire for Test 3: temperature distribution along the horizontal release direction (solid curves) and maximum temperature calculated across the entire domain height at a given distance x (dashed curves).

It has been observed that the horizontal direction of a jet fire causes a significant decrease in "no-harm" hazard distance by temperature due to the buoyancy of combustion products. It is fundamental to know if longer distances should be ensured to avoid harm by thermal radiation from the jet fire. The following harm criteria [3] are used to assess the hazard distances from jet fire by thermal radiation:

- "100% lethality" in 1 min: 25.0 kW/m^2.
- "Second-degree burn" after 20 s: 9.5 kW/m^2.
- "First-degree burn": 4.0 kW/m^2.
- "No-harm" for long exposures: 1.6 kW/m^2.

Simulations with a relative humidity equal to 77% are considered, as more representative of the open atmosphere conditions. The zones designed by limits for "100% lethality" in 1 minute (25.0 kW/m^2) and "second degree burns" after 20 seconds (9.5 kW/m^2) follow the distribution of the flame and combustion products (see Fig. 6). It is expected that in these areas along the tilting flame axis, the convective and conductive heat flux associated with the high temperature combustion products and hot currents overcomes the radiative heat flux. On the other hand, simulation results showed that the "no-harm" by the radiation limit of 1.6 kW/m^2 and the "first-degree burn" limit (4.0 kW/m^2) are reached at the indicated axial distance regardless of the height of the target, whereas it was seen that temperature along the release direction would decay to "no-harm" level within x=1.15L_f (1.75 m). Therefore, Table 6 reports only the hazard distances along the release direction associated to "no-harm" and "first-degree burn" criteria. Considering results for Test 3, it can be observed that the axial "no-harm" distance is equal to 4.75 m (x=3.2L_f). This hazard distance is larger to that obtained along the tilting flame axis for the no-harm level by the temperature of hot gases (3.3 m), i.e. x=2.2L_f. Consistent distances are obtained for the other three tests (x=3.0-3.2L_f). The "no-harm" distance on the sides of the jet fire reaches the domain boundaries (2.7m) for all tests, preventing a throughout analysis and comparison. Overall, it can be concluded that for the horizontal jet fires under investigation the distances along the jet axis associated with the thermal radiation "no-harm" criterion resulted to be longer than those calculated by "no-harm" criterion by temperature. The CFD model is showed to be an accurate tool to predict thermal radiation from a hydrogen jet fire. This should be harmonised with the development of

a reduced tool for an accurate and faster assessment. To the authors' knowledge, no such tool is available in the literature. Further research should be performed in this direction.

Table 6. Hazard distances by thermal radiation from the jet fire perpendicularly to the direction of the release (radial) and along the release direction (axial).

Harm level	"100% lethality" in 1 min: 25.0 kW/m^2	"Second-degree burn" after 20 s: 9.5 kW/m^2	"First-degree burn": 4.0 kW/m^2		"No-harm" for long exposures: 1.6 kW/m^2	
Direction	Radial	Radial	Radial	Axial	Radial	Axial
Test 3	0.31	0.48	0.90	3.19	2.70*	4.75
Test 4	0.39	0.60	0.83	3.42	2.70*	5.26
Test 5	0.29	0.52	0.82	3.11	2.70*	4.77
Test 6	0.32	0.57	0.84	3.06	2.70*	5.10

Note: * - 2.70 m is the distance where the domain boundary is located.

A final analysis addresses the calculation of hazard distances through evaluation of the thermal dose. The assessment is conducted on the sides of the jet fire, as it is expected that in this zone thermal radiative heat flux will be dominant to the convective and conductive heat fluxes associated with the high-temperature combustion products. The thermal dose is a comprehensive parameter calculating the level of harm as a function of the exposure duration (t, s) in addition to the incident thermal radiation (I, kW/m^2). It is expressed in terms of thermal dose (TD) measured in [(kW/m^2)$^{4/3}$s]:

$$TD = \int_0^t I(t)^{4/3}\, dt\,. \tag{1}$$

Thermal dose harm levels for infrared radiation are considered [3] being more conservative and indicated for water vapour emitted thermal radiation [30]. A thermal dose range of 870-2640 (kW/m^2)$^{4/3}$s is indicated for third-degree burns, 240-730 (kW/m^2)$^{4/3}$s for second-degree burns and 80-130 (kW/m^2)$^{4/3}$s for first-degree burns. Table 6 shows that a person located at 0.31 m from the jet axis would incur into "100% lethality", i.e. 78-100% of burned body area [11], if exposed to 25 kW/m^2 for 1 minute to the jet fire in Test 3. This corresponds to TD=4386 (kW/m^2)$^{4/3}$s, which is well beyond the thermal dose range for third-degree burns. Simulation results suggest that the exposure time to 25 kW/m^2 shall be below 25 seconds to not incur third-degree burns. At 0.48 m from the jet fire, second-degree burns are expected after 20 s exposure to 9.5 kW/m^2 (TD=402 (kW/m^2)$^{4/3}$s) and their occurrence could be prevented if exposure is less than 17 s. If the exposure time is prolonged to about 60 s, third-degree burns would occur. Finally, thermal dose calculation at 0.90 m from the jet suggests that the exposure time to a radiation level of 4.0 kW/m^2 should be minor than 17 s to not incur into first-degree burns and 60 s to prevent second-degree burns. The thermal dose is a valuable tool to assess the feasibility of short-term activities and emergency operations, e.g. opening/closing valves, rescue operations, etc. Operators or emergency personnel wearing standard workwear have similar tolerance to radiative heat flux of people not wearing protecting clothes [31]. Thus, distances and exposure time identified above maintain their validity. Firefighters responding to a fire will wear thermal protective clothing, increasing the tolerable levels of radiative heat flux. Authors of the study [31] indicated that 168 s is the tolerance time for pain for a standing firefighter exposed to heat fluxes up to 4.6 kW/m^2. The simulation results show that for Test 3 firefighters can stay as close as 0.71 m from the jet axis to not incur pain, receiving a thermal dose of approximately 1285 (kW/m^2)$^{4/3}$s. A limit of 6.3 kW/m^2 is given for an operating time of 5 minutes if firefighters are wearing aluminised clothing (TD≈3490 (kW/m^2)$^{4/3}$s), reducing further the distance from the jet axis to about 0.59 m.

CONCLUSIONS

The originality of this study includes the numerical investigation of the effect of conjugate heat transfer through a pipe wall on the flow of cryogenic hydrogen and ultimately on the thermal hazards from the resulting jet fires using the validated CFD model. The under-expanded jet theory without pressure losses and heat transfer was found to reproduce experimentally measured mass flow rate with an accuracy of ±15% for releases at ambient temperature. However, the approach was found to be not accurate for

cryogenic releases, leading to overestimations up to 37%. The heat transfer in simulations was seen to cause an increase of temperature from 67 K to 98-127 K at the real nozzle exit depending on the storage pressure and nozzle diameter. A parametric study was conducted to estimate the inlet temperature in the simulated release pipe leading to same mass flow rate as in experiments. Calculated hydrogen parameters at the real nozzle exit were used to define parameters at the notional nozzle exit used as hydrogen release source in simulations of jet fires. The used CFD model was previously validated for vertical hydrogen jet fires with pressure up to 0.5 MPa and temperature within 48-82 K. *The rigour* of this study is established by the expansion of the CFD model validation range against four unique experiments on cryogenic hydrogen horizontal jet fires with release pressure up to 2 MPa and temperature of 80 K. Overall, the trend of radiative heat flux distribution aside the jet axis was well reproduced by simulations. Tests with release diameter equal to 2 mm (pressure up to 2 MPa) and 4 mm (pressure equal to 0.3 MPa) were well reproduced. Prediction accuracy is within 10% for the test at cryogenic storage pressure 1.4 MPa, with exception of few sensors located close to the jet axis. Accuracy for the test with pressure 2 MPa is within 20%. In both tests, the experimental radiative heat flux was underestimated at the further distance from the jet axis (125 cm). Predictive capability for the test with nozzle diameter 4 mm and pressure 0.4 MPa improved when a relative humidity equal to 50% was employed. The experimental flame length was predicted by simulations with very good accuracy (± 15%). Simulations in dry air resulted in a significant increase of radiative heat flux compared to the case with Rh=77%, showing that the effect increases with distance.

The significance of the work is given by the provision of a contemporary validated CFD tool to assess thermal hazards from cryogenic jet fires and avoid over-conservative hazard distances. It is seen that engineering correlations available in the literature to predict hazard distances by harmful temperatures may not be suited for the horizontal hydrogen jet fires. The buoyancy of combustion products has a positive effect on the reduction of the "no harm" distance from x=3.5L_f to x=2.2L_f for vertical and horizontal jet fires respectively. Thermal radiation leads to longer "no-harm" distances in the direction of the jet (x=3.0-3. 2L_f) compared to hazard distance defined by the temperature. Harmful distances on the side of the investigated jets were calculated to be longer than the domain size, i.e. 2.7 m. The assessment of thermal dose on the sides of the jet fire showed that firefighters can stand without harm as close as 0.71 m to a jet fire axis for no longer than 168 s. Overall, it is concluded that a throughout assessment of thermal hazards and associated distances from a hydrogen jet fire should combine the analysis of temperature, thermal radiation and thermal dose, as they were found to be complementary.

ACKNOWLEDGEMENTS

This research has received funding from the Fuel Cells and Hydrogen 2 Joint Undertaking under grant agreement No.779613 (PRESLHY), No.736648 (NET-Tools), No.826193 (HyTunnel-CS) and No.875089 (HyResponder). This Joint Undertaking receives support from the European Union's Horizon 2020 research and innovation programme, Hydrogen Europe and Hydrogen Europe research.

REFERENCES

[1] DOE. Technical Assessment: Cryo-compressed hydrogen storage for vehicular applications 2006.

[2] Friedrich A, Breitung W, Stern G, Veser A, Kuznetsov M, Fast G, et al. Ignition and heat radiation of cryogenic hydrogen jets. Int J Hydrogen Energy 2012;37:17589–98.

[3] Lachance J, Tchouvelev A, Engebo A. Development of uniform harm criteria for use in quantitative risk analysis of the hydrogen infrastructure. Int J Hydrogen Energy 2011;36:2381–8.

[4] Panda PP, Hecht ES. Ignition and flame characteristics of cryogenic hydrogen releases. Int J Hydrogen Energy 2017;42:775–85.

[5] Kuznetsov M, Pariset S, Friedrich A, Stern G, Travis J, Jordan T. Experimental investigation of non-ideality and non-adiabatic effects under high pressure releases. Int J Hydrogen Energy 2015.

[6] Cirrone DMC, Makarov D, Molkov V. Thermal radiation from cryogenic hydrogen jet fires. Int J Hydrogen Energy 2019;44:8874–85.

[7] Molkov V. Fundamentals of Hydrogen Safety Engineering I, Download at bookboon.com, 2012.

[8] Hall JE, Hooker P, Willoughby D. Ignited releases of liquid hydrogen: Safety considerations of thermal and overpressure effects. Int J Hydrogen Energy 2014;39:20547–53.

[9] Cirrone D, Makarov D, Molkov V. Near Field Thermal Dose of Cryogenic Hydrogen Jet Fires. oceedings Ninth Int. Semin. Fire Explos. Hazards, 2019, p. 1360–6.

[10] Breitung W, Stern G, Veser A, Friedrich A, Kutznetsov M, Fast G, et al. Final Report:Experimental and theoretical investigations of sonic hydrogen discharge and jet flames from small breaks. 2009.

[11] LaChance JL. Progress in risk assessment methodologies for emerging hydrogen applications. 6th Int. Short Course "Progress Hydrog. Saf. – Regul. codes Stand., Belfast, UK: 2010.

[12] Molkov V, Makarov V, Bragin M V. Physics and modelling of underexpanded jets and hydrogen dispersion in atmosphere. Phys Extrem States Matter 2009:146–9.

[13] Cirrone D, Makarov D, Molkov V. Cryogenic hydrogen jets: flammable envelope size and hazard distances for jet fire. Int. Conf. Hydrog. Saf., Adelaide, Australia: 2019.

[14] Smagorinsky J. General circulation experiments with the primitive equations. I. The basic experiment. Mon Weather Rev 1963;3:99–164.

[15] Bell IH, Wronski J, Quoilin S, Lemort V. Pure and Pseudo-pure Fluid Thermophysical Property Evaluation and the Open-Source Thermophysical Property Library CoolProp. Ind Eng Chem Res 2014;53:2498–508.

[16] Taira Y, Saburi T, Kubota S, Sugiyama Y, Matsuo A. Numerical investigation of hydrogen leakage from a high pressure tank and its explosion. Int. Conf. Hydrog. Saf., Yokohama, Japan: 2015.

[17] Properties of materials, http://www.caffnib.co.uk/properties.html (accessed 30.09.2020).

[18] Shih TH, Liou WW, Yang A, Shabbir Z. A new eddy-viscosity model for high Reynolds number turbulent flows—model development and validation. Comput Fluids 1995;24:227–238.

[19] Magnussen B. On the structure of turbulence and a generalized eddy dissipation concept for chemical reaction in turbulent flow. Am Inst Aeronaut Astronaut 1981.

[20] Molkov V, Shentsov V, Brennan S, Makarov D. Hydrogen non-premixed combustion in enclosure with one vent and sustained release: Numerical experiments. Int J Hydrog Energy 2014;39:10788–10801.

[21] Murthy JY, Mathur SR. A finite volume method for radiative heat transfer using unstructured meshes. 36th AIAA Aerosp Sci Meet Exhib 1998.

[22] Hubbard C., Tien GL. Infrared Mean Absorption Coefficients of Luminous Flames and Smoke. J Heat Transf 1978;100:235–239.

[23] Omega. Emissivity of common materials. www.omega.com (accessed 15.02.2017).

[24] Weather&Climate. Average Humidity In Karlsruhe (Baden-Württemberg) 2020. https://weather-and-climate.com/average-monthly-Humidity-perc,karlsruhe,Germany (accessed 15.10.2020).

[25] Ekoto IW, Ruggles AJ, Creitz LW, Li JX. Updated jet flame radiation modeling with buoyancy corrections. Int J Hydrogen Energy 2014;39:20570–7.

[26] Schefer R, Houf B, Bourne B, Colton J. Experimental Measurements to Characterize the Thermal and Radiation Properties of an Open-flame Hydrogen Plume. Proc 15th Annu Hydrog Conf Hydrog Expo, 2004.

[27] Yates D. Innovative solutions to reduce separation distances in on-board hydrogen storage. PhD Thesis. 2016.

[28] Barlow RS, Carter CD. Relationship among nitric oxide, temperature and mixture fraction in hydrogen jet flames. Combust Flame 1996;104:288–99.

[29] Imamura T, Hamada S, Mogi T, Wada Y, Horiguchi S, Miyake A, et al. Experimental investigation on the thermal properties of hydrogen jet flame and hot currents in the downstream region. Int J Hydrogen Energy 2008;33:3426–35.

[30] Howell JR, Mengüc MP, Siegel R. Thermal Radiation Heat Transfer. 6th Editio. Taylor and Francis Group; 2016.

[31] Heus R, Denhartog EA. Maximum allowable exposure to different heat radiation levels in three types of heat protective clothing. Ind Health 2017;55:529–36.